An analysis of control using the weighted sum of spatial gradients in active structural acoustic control for flat panels

Yin Cao,[1] Scott. D. Sommerfeldt,[1] William Johnson,[2] Jonathan D. Blotter,[2,a)] and Pegah Ashlani[1]

[1]Department of Physics and Astronomy, Brigham Young University, Provo, Utah 84602, USA
[2]Department of Mechanical Engineering, Brigham Young University, Provo, Utah 84602, USA

Active structural acoustic control uses a control metric that when minimized reduces the radiated sound. Previous research has identified the weighted sum of spatial gradients (WSSG) control metric and has shown that it is effective in attenuating the radiated sound power from a plate. The WSSG control metric is computed using weighted measurements of the structural response from four closely spaced accelerometers. In this work, it is shown that the weights used to compute WSSG directly impact the control performance and further understanding into choosing appropriate weights is presented. Weights optimized for single frequencies are investigated and shown to achieve nearly the same performance as minimizing sound power. A set of parameter-based weights for broadband frequency control is also proposed and analyzed. These parameter-based weights are inversely proportional to the square of the flexural wavenumber and can be computed using the ratio of the flexural rigidity to the mass per unit area. Both numerical and experimental results are presented using parameter-based weights for simply supported and clamped plates. The results show that the WSSG control using parameter-based weights is easy to implement and works more effectively than previous methods. © 2015 Acoustical Society of America.
[http://dx.doi.org/10.1121/1.4934730]

I. INTRODUCTION

Active control of structure borne sound using structural control sources is referred to as active structural acoustic control (ASAC) and offers several advantages in practical applications. ASAC was introduced in the 1990s and since that time considerable research has been reported.[1–8] A key issue in ASAC is how to accurately sense the radiated acoustic power using real-time structural sensors. Minimizing volume velocity has been proposed and investigated by numerous researchers.[9–16] Volume velocity provides a good estimation of the amplitude of the lowest-order radiation mode at frequencies where the structure is smaller than the acoustic wavelength. The advantages of this method are that volume velocity can be measured using an array of evenly distributed point sensors or using specialized shaped polyvinylidene fluoride (PVDF) sensors. The drawbacks are that it often requires a large number of sensors, and the control approach becomes significantly less effective at higher frequencies.

To control specific radiation modes of the structure, some researchers proposed using a radiation modal filter.[17–20] Designing a radiation modal filter usually requires some *a priori* knowledge of the geometry, which also means the radiation modal filter requires a unique design for different structures. Other researchers developed a method called discrete structural acoustic sensing, which does not use radiation mode information but still relies on *a prior* knowledge

of the transfer function from the vibration field to the pressure field.[21–24] Radiation clusters were proposed as a further improvement to minimizing volume velocity.[25,26] With this approach, the structural modes are divided into even and odd modes. The even modes correspond to a set of volume velocity related modes, and odd modes correspond to a set of non-volume velocity related modes. When controlling high frequency noise, even and odd modes should both be incorporated into the cost function, while only even modes should be incorporated into the cost function when controlling low frequency noise.

Recently, a new control metric called the weighted sum of spatial gradients (WSSG), which is based on measurements from four closely spaced accelerometers, was investigated and shown to significantly attenuate the radiated sound power.[27] WSSG consists of the weighted sum of the squared displacement field, w, and the squared spatial derivatives, $\partial w/\partial x$, $\partial w/\partial y$, and $\partial^2 w/\partial x\partial y$. Fisher *et al.* showed through computer simulation that on a simply supported plate, WSSG has less dependency on sensor location and is able to provide better overall radiated sound power attenuation levels than minimizing either volume velocity or structural intensity.[27] In addition, it was found that the weights applied to the four quantities have an impact on the sound power attenuation.

In this paper, the properties of WSSG are analyzed in more detail. The optimized weights for a single frequency are obtained through a simulated annealing method, and the corresponding control effect is shown to be nearly as good as minimizing the sound power. The weights for broadband

excitation are also examined. A method to determine the broadband weights based on the structural material and geometry is proposed and shown to have promise for a simple practical implementation. Experimental results from applying WSSG to flat rectangular simply supported and clamped plates are presented and discussed. It is shown that the WSSG technique is a universal and easily implemented method and can effectively attenuate the radiated noise from vibrating flat rectangular plates. In Sec. II, a brief overview of the WSSG plate model is presented. In Secs. III and IV, simulated and experimental results are presented and compared. The main conclusions are summarized in Sec. V.

II. THEORY

A. Dynamic model of the plate

The equations describing the vibration of both a simply supported plate and a clamped plate are briefly reviewed here for completeness. The governing equation for a vibrating plate is given by

$$D\left(\frac{\partial^4}{\partial x^4}+2\frac{\partial^4}{\partial x^2 \partial y^2}+\frac{\partial^4}{\partial y^4}\right)w(x,y)-\bar{m}\omega^2 w(x,y)=F(x,y),$$

(1)

where D is the bending stiffness, w is the transverse displacement, $\bar{m}$ is the mass per unit area, ω is the excitation frequency, and F is the amplitude of the force excitation.[28] The plate excitation is assumed to be time harmonic; therefore the displacement and force expressions can be assumed to be multiplied by $e^{j\omega t}$, although not shown explicitly. This is an assumption made throughout the remainder of this paper. Also, for the current formulation, the plate will be assumed to be excited by an array of point forces, so that $F(x,y) = \sum_q f_q \delta(x-x_q)\delta(y-y_q)$, with f_q indicating the q th applied force as a complex number, $\delta(\cdot)$ the Dirac delta function, and x_q and y_q the location of the q th force.

The transverse displacement of the simply supported plate is given by[6]

$$w(x,y)=\sum_q \frac{f_q}{\rho h}\sum_m^\infty\sum_n^\infty\frac{W_{mn}(x,y)W_{mn}(x_0,y_0)}{\left[\omega_{mn}^2(1+j\eta)-\omega^2\right]},$$

(2)

where

$$W_{mn}(x,y)=\frac{2}{\sqrt{L_x L_y}}\sin\left(\frac{m\pi x}{L_x}\right)\sin\left(\frac{n\pi y}{L_y}\right)$$

(3)

and

$$\omega_{mn}=\sqrt{\frac{D}{\rho h}}\left[\left(\frac{m\pi}{L_x}\right)^2+\left(\frac{n\pi}{L_y}\right)^2\right].$$

(4)

In Eqs. (2)–(4), ρ is the density of the plate, h is the thickness of the plate, and η is the modal damping ratio. L_x and L_y are the x and y dimensions of the plate. The bending stiffness, D, is given by $Eh^3/12(1-\nu^2)$ where E is Young's modulus and ν is Poisson's ratio.

Although an exact analytical solution to Eq. (1) for clamped rectangular plates is not available, a method assuming

the product of beam mode shapes as the eigenfunctions of the plate can be used to provide an approximate analytical solution,[29] which is given by

$$w(x,y)=\sum_q f_q\sum_m^\infty\sum_n^\infty\frac{X_m(x_q)Y_n(y_q)X_m(x)Y_n(y)}{D(I_1 I_2+2I_3 I_4+I_5 I_6)-\bar{m}\omega^2 I_2 I_6},$$

(5)

where

$$X_m(x)=J\left(\frac{\lambda_m x}{L_x}\right)-\frac{J(\lambda_m)}{H(\lambda_m)}H\left(\frac{\lambda_m x}{L_x}\right),$$

(6)

$$Y_n(y)=J\left(\frac{\lambda_n y}{L_y}\right)-\frac{J(\lambda_n)}{H(\lambda_n)}H\left(\frac{\lambda_n y}{L_y}\right),$$

(7)

$$J(u)=\cosh(u)-\cos(u),$$

(8)

$$H(u)=\sinh(u)-\sin(u).$$

(9)

The subscripts m and n indicate structural mode numbers, and the values for λ_m and λ_n, the eigenvalues of the system, satisfy

$$\cosh(\lambda)\cos(\lambda)=1.$$

(10)

Also

$$I_1=\int_0^{L_x}X_m^{(4)}(x)X_m(x)dx,\quad I_2=\int_0^{L_y}Y_n^2(y)dy,$$

$$I_3=\int_0^{L_x}X''_m(x)X_m(x)dx,\quad I_4=\int_0^{L_y}Y''_n(y)Y_n(y)dy,$$

$$I_5=\int_0^{L_y}Y_n^{(4)}(y)Y_n(y)dy,\quad I_6=\int_0^{L_x}X_m^2(x)dx.$$

(11)

$X_m(\cdot)$ and $Y_n(\cdot)$ are the assumed shape functions, and $X''_m(\cdot)$, $Y''_n(\cdot)$ and $X_m^{(4)}(\cdot)$, $Y_n^{(4)}(\cdot)$ refer to the second and fourth spatial derivatives, respectively. This method has been verified and shown to accurately predict the natural frequencies when compared to the Rayleigh–Ritz method and experimental results for a clamped rectangular plate.[30]

In this paper, the radiated sound power for both theoretical and experimental results is obtained using the method of elementary radiators and the radiation resistance matrix.[31] The radiation resistance matrix discretizes the plate geometry and provides a simplified and computationally more efficient method for calculating the radiated sound power at low frequencies. It is derived by discretizing the plate into elemental radiators and calculating the mutual radiation impedances between each elemental radiator and all others. This matrix is given, for a rectangular plate,[31] by

$$\mathbf{R}(\omega)=\frac{\omega^2\rho_0\Delta S^2}{4\pi c_0}\begin{bmatrix}1 & \frac{\sin(k_0 r_{12})}{k_0 r_{12}} & \cdots & \frac{\sin(k_0 r_{1I})}{k_0 r_{1I}}\\ \frac{\sin(k_0 r_{21})}{k_0 r_{21}} & 1 & \cdots & \vdots\\ \vdots & \vdots & \ddots & \vdots\\ \frac{\sin(k_0 r_{I1})}{k_0 r_{I1}} & \cdots & \cdots & 1\end{bmatrix},$$

(12)

where ρ_0 and c_0 are the density and the sound velocity of air, respectively, r_{ij} is the distance between the i th element and the j th element, k_0 is the acoustic wavenumber in air, and ΔS is the area of each element. Using the radiation resistance matrix, the sound power is calculated as

$$\Pi(\omega) = \mathbf{v}_e^H(\omega)\mathbf{R}(\omega)\mathbf{v}_e(\omega), \tag{13}$$

where $\mathbf{v}_e$ is a vector containing the velocity of each elemental radiator, and $(\cdot)^H$ signifies the Hermitian transpose.

B. Review of the WSSG theory

In this section, a brief overview of WSSG is provided. A more complete derivation is given by Fisher *et al.*[27] The original concept of WSSG was developed with two objectives. The first was that the control metric be as spatially uniform as possible. This largely eliminates the sensitivity of the performance on the error sensor location and would require no prior knowledge of the structure. The second objective was that the control metric should be correlated with the sound power radiation, so that minimizing WSSG would result in attenuating radiated sound power.

It was noted by Fisher *et al.*[27] that the weighted combination of the four squared quantities, namely, the transverse displacement w and the spatial derivatives $\partial w/\partial x$, $\partial w/\partial y$, and $\partial^2 w/\partial x\partial y$, has the potential to fulfill these two objectives. WSSG was thus defined as the weighted summation of these four terms, each multiplied by a weighting value (α, β, γ, δ), so that a spatially uniform value can be formed, as shown in Eq. (14) by

$$\text{WSSG} = \alpha(w)^2 + \beta\left(\frac{\partial w}{\partial x}\right)^2 + \gamma\left(\frac{\partial w}{\partial y}\right)^2 + \delta\left(\frac{\partial^2 w}{\partial x\partial y}\right)^2. \tag{14}$$

While w represents the displacement in these terms, it should be noted that for time harmonic excitation sources, velocity or acceleration could equally be used.

One way to define the weights is in terms of the structural wavenumber. The wavenumber components of a simply supported plate in the x and y directions are $k_m = m\pi/L_x$ and $k_n = n\pi/L_y$, respectively. For a clamped plate, the components in the x and y directions are $k_m = \lambda_m/L_x$ and $k_n = \lambda_n/L_y$, where λ_m, λ_n are calculated through Eq. (10). It can be shown that once the weights are chosen for each resonance frequency as

$$\alpha = 1, \quad \beta = \left(\frac{1}{k_m}\right)^2, \quad \gamma = \left(\frac{1}{k_n}\right)^2, \quad \delta = \left(\frac{1}{k_m k_n}\right)^2, \tag{15}$$

the WSSG field will have high spatial uniformity. This general expression is significant because it shows that each term is weighted by the corresponding wavenumber components and allows for the selection of weights on plates with non-ideal boundary condition or non-ideal shapes if the wavenumber components in x and y can be determined.

It is also recognized that the gradients associated with the four terms of WSSG have noticeable similarities to the global spatial properties of the first four radiation modes. It is hypothesized that this similarity is connected with the observed behavior that allows for a single or local measurement on the plate to control the radiation mode shapes globally as opposed to volume velocity, which requires a global measurement of the plate to control the first radiation mode. These similarities suggest that WSSG may be effective at targeting the first four radiation mode shapes for a plate and will therefore be a good candidate for use in ASAC. It is noted that WSSG is a local "point" measurement, while radiated sound power is a global property, so it is improper to say that there is a direct correlation between WSSG and the radiated sound power. However, the four terms of WSSG do correspond to the patterns associated with the first four radiation mode shapes; this leads to the hypothesis that minimizing WSSG generally results in an attenuation of the radiated sound power.

III. ANALYTICAL ANALYSIS AND SIMULATIONS

This section provides an analytical investigation of four methods to compute the WSSG weights shown in Eqs. (14) and (15). Insights regarding these methods are discussed. Properties of the simply supported and the clamped plates used in the following analysis are listed in Table I. Several different disturbance, control, and sensor locations as described by Table II are investigated.

A. Averaged weights for broadband frequency

Two methods of the four methods for calculating the weights are presented in this section. The first method is frequency dependent and uses the weights of the nearest resonance frequency according to Eq. (15); the second method uses a constant set of weights, which are obtained by averaging all of the weights corresponding to every mode in the frequency range of interest. In this work, all resonances in the frequency range from 0 to 500 Hz are included in this average. Actuator and sensor locations described in Table II are used. While results will be shown for specific error sensor locations, it has been observed that the attenuation achieved for different sensor locations is nearly constant. Figure 1 shows the simulation control results for the simply supported plate and the clamped plate, respectively. In Fig. 1, it is shown that frequency dependent weights and averaged weights both provide good control across the whole frequency range. Furthermore, there is generally relatively little difference between the two methods. This implies that the

TABLE I. Properties of the simply supported and clamped plates.

Property	Value
Length (x direction)(L_x) (m)	0.473
Length (y direction)(L_y) (m)	0.753
Thickness (h) (m)	0.003
Young's modulus (E) (GPa)	68.9
Poisson's ratio (ν)	0.334
Density (ρ) (kg/m^3)	2700
Damping ratio (η) (%)	1

TABLE II. Coordinates for the actuator and sensor locations.

Actuator/Sensor	Configuration one location (x, y) (m)
Disturbance	(0.445, 0.692)
Controller one	(0.422, 0.064)
Sensor	(0.245, 0.285)
Controller two (if applicable)	(0.230, 0.650)

weights used in WSSG are fairly robust and determining the exact optimal values of the weights may not be critical to achieve good performance.

Although the attenuation shown in Fig. 1(a) is significant at many resonance frequencies, there is very little attenuation achieved at 255 and 375 Hz. At these frequencies, multiple closely spaced structural modes occur. Because the frequencies of these modes are so close to each other, the individual mode shapes superimpose on top of each other and cause distortions in the resulting structural response. These degenerate modes essentially add additional degrees of freedom of motion to the plate.[32] Thus there are more degrees of freedom than degrees of control.

It is shown in Fig. 1(a) that by adding a second control shaker, the two degenerate modes at 255 Hz are effectively

controlled. There are actually three degenerate modes around 375 Hz, and it is shown that two control shakers cannot control these three modes. Results similar to Fig. 1(a) were observed for several different configurations. Therefore adding another control shaker is an effective way to control the degenerate mode if there are multiple closely spaced modes contributing to the radiated sound power.
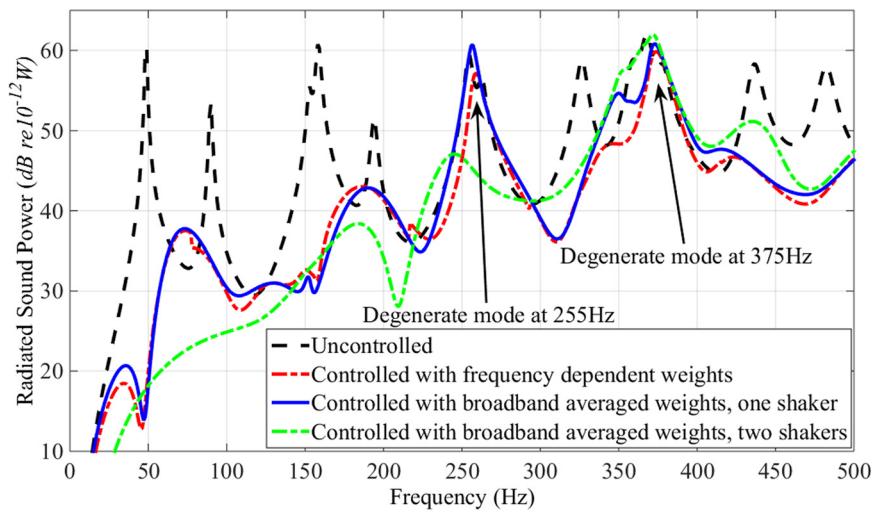
B. Optimized weights for a single frequency

In Fig. 1, there is some amplification of the radiated sound power at some off resonance frequencies. To determine the optimum weights used in WSSG for attenuating radiated sound power and obtain the best control results WSSG can achieve, a simple optimization problem was defined as
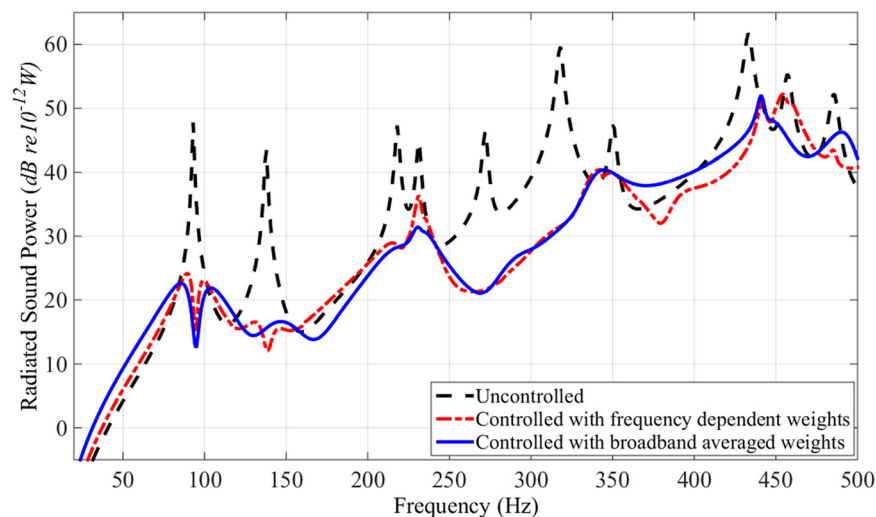
$$\min_{\alpha, \beta, \gamma, \delta} (\text{Sound Radiation Power After Control})$$

$$\text{subject to} : [\alpha, \beta, \gamma, \delta] \in [0, 1].$$

The simulated annealing method is adopted to solve this global optimization problem. Simulated annealing was implemented in MATLAB using the *simulannealbnd* function.

FIG. 1. (Color online) Radiated sound power for two methods of calculating the WSSG weights. Dashed: uncontrolled sound power; dash dotted: controlled with frequency dependent weights; solid: controlled with averaged weights. (a) Simply supported plate, (b) clamped plate.

J. Acoust. Soc. Am. **138** (5), November 2015

Cao *et al.* 2989

The reason for restricting the weights to the range between 0 and 1 is that it is a normalized value. Figure 2 shows the comparison of the control results by minimizing sound power and by minimizing WSSG using the optimized weights obtained through the simulated annealing method for the simply supported and the clamped plate, respectively. It can be seen from Fig. 2 that by using simulated annealing to determine the optimized weights at each frequency, WSSG is able to perform essentially as well as minimizing the sound power for this configuration. This means that if the optimized weights are found for each frequency, WSSG (which only uses four accelerometers) can be used to maximize the attenuation of radiated sound power. During the simulation process, it was also found that using only the first three terms of WSSG, as compared to using all four terms of WSSG, can be used to obtain good control results as shown in Fig. 2. This indicates that the fourth term is not necessary to use in WSSG, at least for these conditions. It will be shown in Sec. III C that the fourth term in the WSSG expression can contain significant noise due to the derivatives of experimental data. Therefore in the following analysis, the fourth term of WSSG will not be used.

C. Parameter-based weights for broadband frequency

The simulated annealing method is able to find the optimized weights for WSSG at each frequency. However, a simple process to find the optimized weights, rather than using the simulated annealing method, is more preferable in real implementations. Figure 3 shows the first weight, α, calculated through the simulated annealing method, as a function of frequency. It can be seen that the weights obtained at each frequency appear to be random and unsystematic; thus, there is no discernable rule that can be established to determine these optimized weights for each frequency.

In this section, a method to determine the weights for a broadband frequency range, based on parameters of the plate, is presented and analyzed. In the analysis, the first weight, α, is normalized to 1, and the fourth weight is neglected due to the analysis in Sec. III B. Initially several different cases corresponding to different materials and thicknesses of the simply supported plate, but with the same length and width, are examined. Table III shows the parameters of the different simply supported plates. The actuator and sensor locations are the same as in Table II. In Table III,
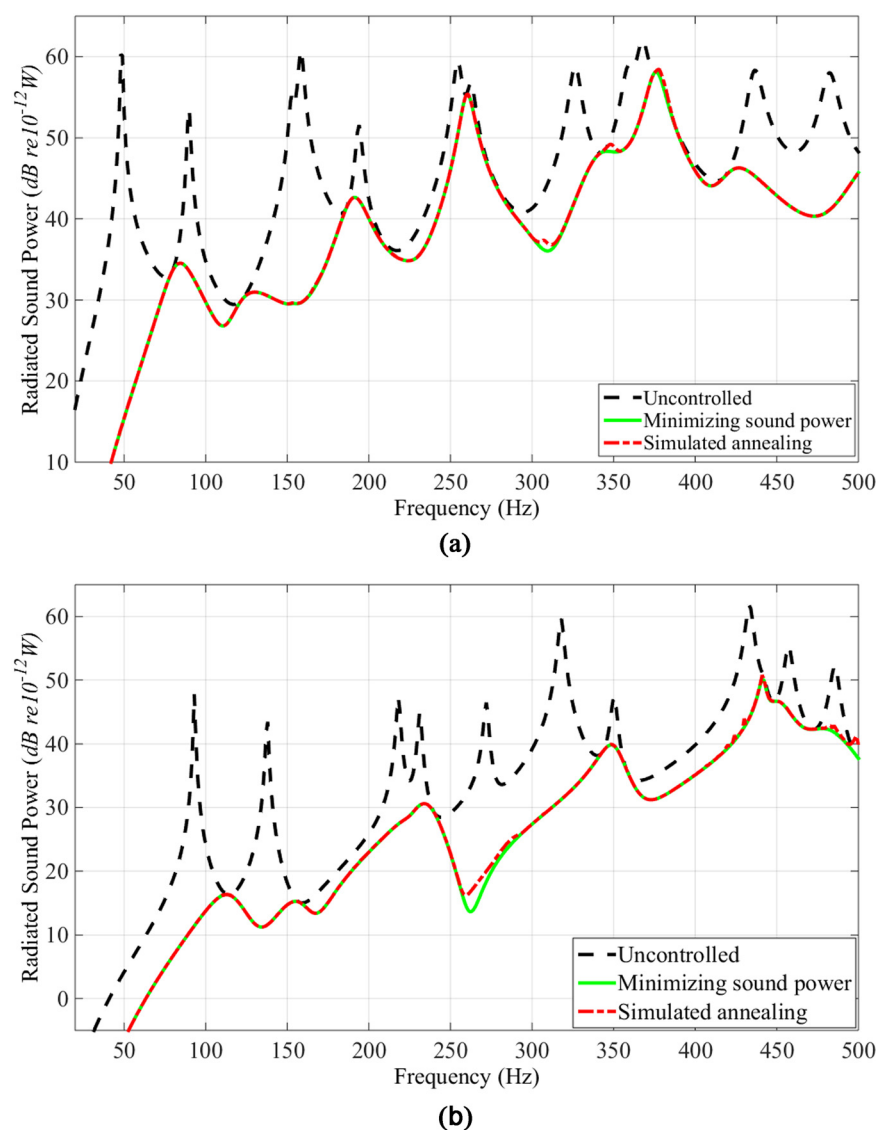

FIG. 2. (Color online) Comparison of plate control results by minimizing sound power and WSSG using the optimized weights obtained through the simulated annealing method. Dashed: uncontrolled sound power; solid: minimizing sound power; dash dotted: WSSG using optimized weights obtained through simulated annealing. (a) Simply supported plate, (b) clamped plate.
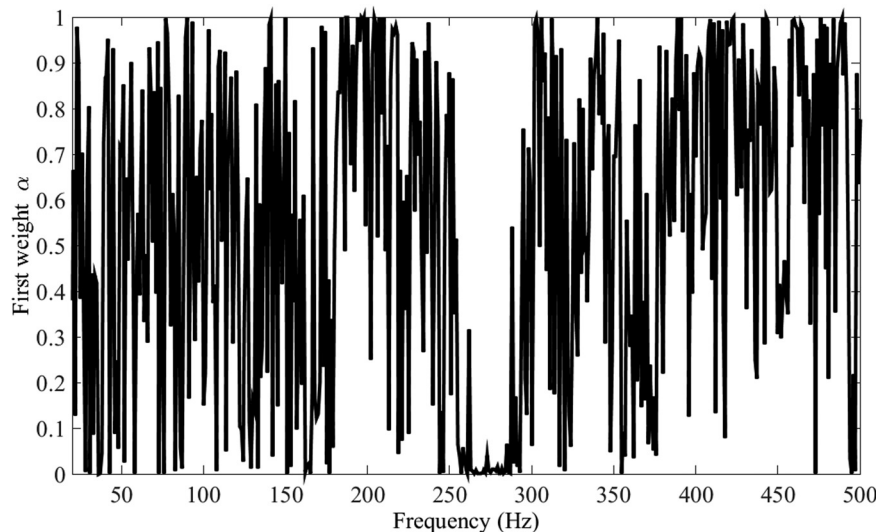
FIG. 3. The first weight obtained through simulated annealing.

the value of $D/\rho h$ is also shown. Given that the wavenumber can be expressed as

$$k_f^2 = \sqrt{\frac{\rho h}{D}}\omega, \qquad (16)$$

it is noted that $\sqrt{D/\rho h}$ is inversely proportional to the square of the transverse wavenumber. As a result, it will be demonstrated later that this ratio of plate parameters can be used in place of the square of the transverse wavenumber to directly determine the proper values of the weights.

Figure 4 shows the total sound power attenuation from 20 to 500 Hz as a function of different weights (plotted on a log scale) with each plot corresponding to different cases shown in Table III. The darker the color, the greater the attenuation achieved. For simplicity, only three cases are plotted; the other three cases have the same trend as those shown. The length and width of the plate for the different cases in Table III are the same as depicted in Table I. On inspection of Fig. 4, the dark region on each figure appears to be somewhat complex. However, the darkest region in each figure has a relatively large area; this means there is a large range of nearly optimized weights. It is again apparent that choosing the exact value of the optimized weights is less critical, once the proper order of magnitude of the weights is determined. Hence in the following analysis, there is little attempt to determine the exact value of the optimized weights. Thus a set of (nearly optimal) parameter-based weights will be identified in the

following analysis. For Fig. 4, the circular points in the figures indicate the weights for the largest attenuation that can be achieved. Table IV shows the optimum weights of different cases, corresponding to the circular points in each of the figures that result in the greatest attenuation of the radiated sound power. It can be seen in Table IV that the increase in the optimum weight values for the different cases corresponds to increasing values of $D/\rho h$. According to Eq. (15), the weights are shown to be inversely proportional to the wavenumber in the x and y directions. In these expressions, it is assumed that the optimum weights are related to the transverse wavenumber; this suggests that if the value of D is known, the parameter-based weights can be obtained using the results provided in Table IV and interpolating as needed for the specific value of $D/\rho h$.

From this analysis, it is assumed that when the value of $D/\rho h$ remains almost the same, the broadband parameter-based weights should remain almost the same. Hence two other cases (simply supported case 7 and clamped case 8), which are shown in Table IV, are considered in the following analysis. These two cases have the same length and width as shown in Table I. Figure 5 shows the corresponding total radiated sound power attenuation as a function of the weights. In Table IV, cases 2 and 7 are both simply supported with $D/\rho h$ equal to 2.52 and 2.39, respectively. Their transverse wavenumbers are similar. Furthermore, it can be seen from Figs. 4(a) and 5(a) that the dependence of the sound power attenuation on the weight values used is very similar, and the parameter-based weights corresponding to the circular point locations are the same. This indicates that the assumption in the preceding text is reasonable. For different boundary conditions but with the same transverse wavenumber, results can be compared using the data of the simply supported case 3 and the clamped case 8 in Table IV and the corresponding plots in Figs. 4(b) and 5(b). Although the figures of the total radiated sound power attenuation as a function of the weights are somewhat different in Figs. 4(b) and 5(b), the dark regions indicating weights that yield near-optimum attenuation are similar in shape and extent. Thus the same parameter-based weights can be used effectively in

TABLE III. Material properties and plate thickness for simply supported cases.

Case	Modulus (Pa)	Density (kg/m³)	Thickness (m)	$D/\rho h$ (m⁴/s²)
1	6.89×10^{10}	10800	0.001	0.60
2	2.1×10^{11}	7800	0.001	2.52
3	6.89×10^{10}	2700	0.002	9.55
4	6.89×10^{10}	2700	0.003	22.92
5	6.89×10^{10}	2700	0.005	59.66
6	6.89×10^{10}	2700	0.020	954.57

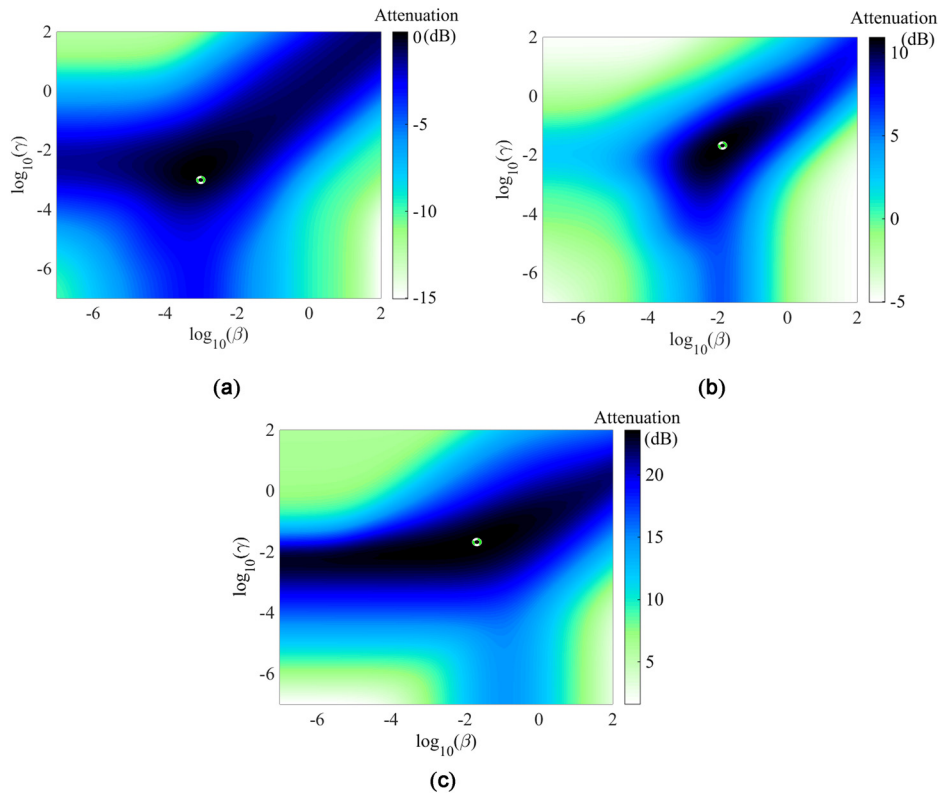J. Acoust. Soc. Am. **138** (5), November 2015

Cao *et al.* 2991

FIG. 4. (Color online) Total radiated sound power attenuation (dB) as a function of different weights for different simply supported plates with the same length and width. (a) case 2, (b) case 3, (c) case 6.

both cases. This further confirms that it is not critical to determine the exact optimal value of the weights but rather the order of magnitude. Therefore a reasonable practical approach is to use the value of $D/\rho h$ to directly determine the parameter-based weights.

To confirm that varying configurations do not significantly change the parameter-based weights, six additional configurations with aspect ratios varying from 1 to 10 and varying sensor and actuator locations were investigated. For these configurations, the value of $D/\rho h$ was fixed to be 2.39, which is the same as case 7. The results are not shown here, but as expected, it was found that the parameter-based weights did not vary appreciably and that the value of $D/\rho h$ can be used to determine the parameter-based weights for broadband frequency excitation.

Finally, the control results using broadband parameter-based weights are compared with results using the averaged weights utilized for Fig. 1. The material properties are the same as in Table I, from which the value of $D/\rho h$ can be calculated to be approximately 24. Thus from Table IV, it can
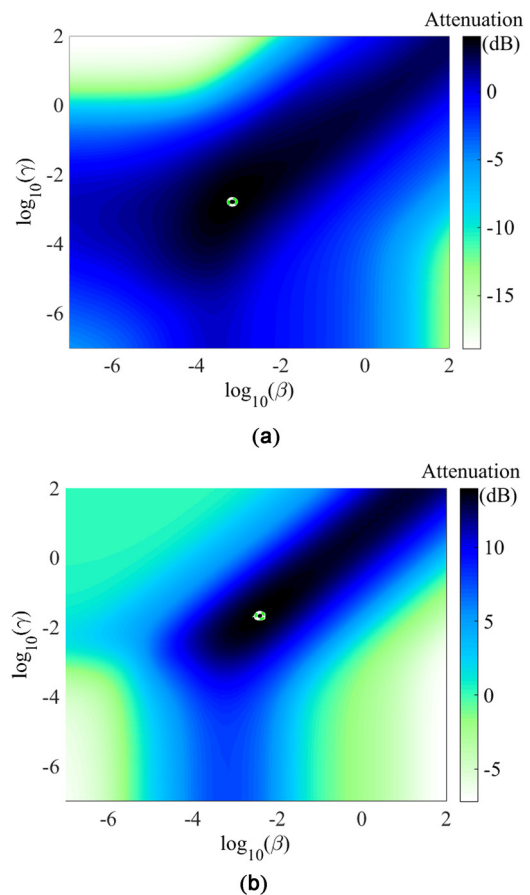

FIG. 5. (Color online) Total radiated sound power attenuation (dB) as a function of different weights for different cases. (a) case 7, (b) case 8.

TABLE IV. Optimized weights for different cases.

Case	Boundary condition	$D/\rho h$	$log_{10}\beta$	$log_{10}\gamma$
1	Simply supported	0.60	−3.14	−3.14
2	Simply supported	2.52	−3.18	−2.78
3	Simply supported	9.55	−1.86	−1.86
4	Simply supported	22.92	−1.86	−1.86
5	Simply supported	59.66	−1.86	−1.67
6	Simply supported	954.57	−1.67	−1.67
7	Simply supported	2.39	−3.14	−2.78
8	Clamped	9.55	−2.16	−1.86

be determined that the parameter-based weights, β and γ, should be 0.014 (converting back from their logarithmic values). Figure 6 shows the control results obtained using parameter-based weights and averaged weights for both the simply supported plate and the clamped plate. For the simply supported plate, it can be seen from Fig. 6(a) that using parameter-based weights provides good control performance except at around 255 and 375 Hz; this is similar to the averaged weights. This has already been identified as being due to degenerate modes. At other frequencies, the attenuation is significant. However, because of the degenerate modes, the total overall attenuation obtained using averaged weights and parameter-based weights is only 2.60 and 4.12 dB, respectively. For the clamped plate, there are no degenerate modes, and almost all of the modes are attenuated significantly. The total overall attenuation obtained using averaged weights and parameter-based weights is 6.55 and 7.82 dB, respectively.

To control the degenerate modes in the simply supported plate, a second shaker is added to control the additional degree of freedom. Figure 6(a) also shows the comparison of control results between averaged weights and parameter-based weights for the simply supported plate using two shakers (dashed line and dotted line). It can be seen that adding a second shaker yields better control performance at the degenerate mode around 255 Hz, as was also shown in Fig. 1(a). For the other degenerate modes around 375 Hz, the parameter-based weights provide better attenuation than the averaged weights. The total overall attenuation for averaged weights and parameter-based weights is 1.98 and 4.23 dB, respectively.

The analysis in the preceding text indicates that effective sound power attenuation across the whole frequency range can be obtained by using the parameter-based weights, which can be directly obtained from the value of $D/\rho h$. It generally provides control performance that is equal to or better than obtained using averaged weights. Although there are still some frequencies at which the parameter-based weights do not perform better than the averaged weights, the total sound power attenuation obtained using parameter-based weights is still a little larger than using averaged weights. Furthermore, it is much easier to determine the parameter-based weights than the averaged weights, which is the real advantage of using parameter-based weights.
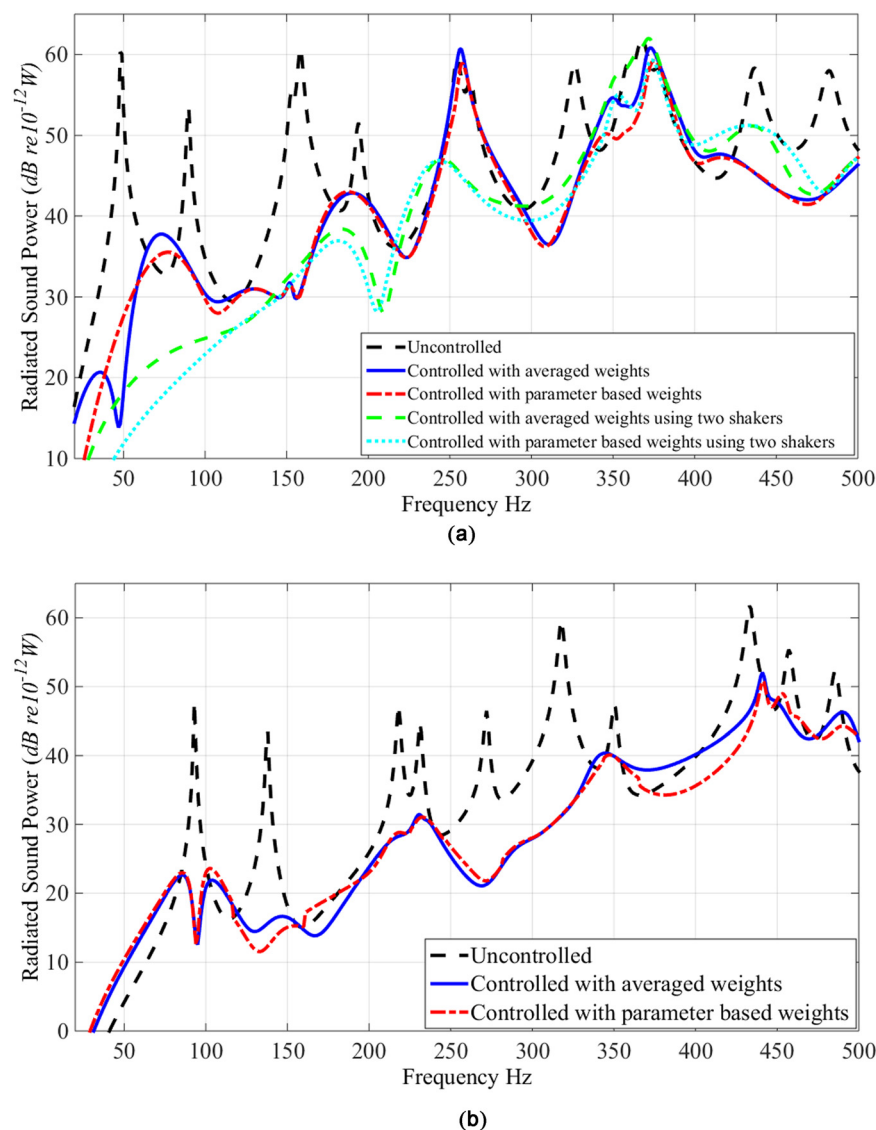

FIG. 6. (Color online) Comparison of control results using averaged weights and parameter-based weights. (a) Simply supported plate, (b) clamped plate.

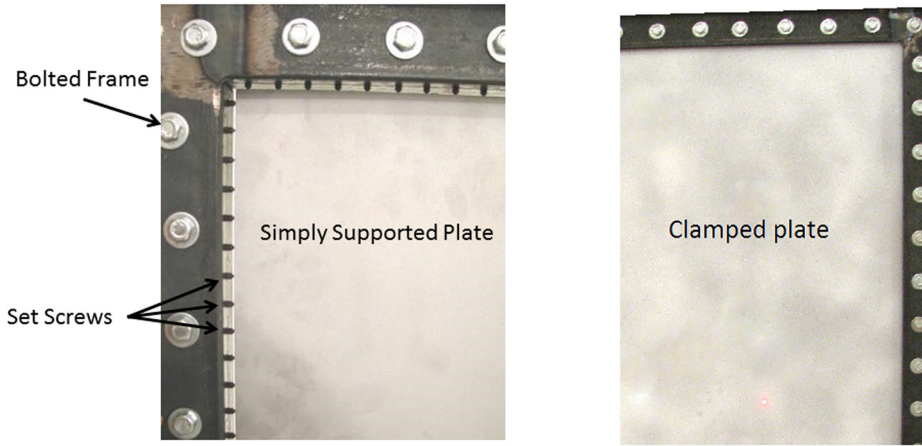J. Acoust. Soc. Am. **138** (5), November 2015

Cao *et al.* 2993

FIG. 7. (Color online) The experimental setup for simply supported and clamped boundary conditions.

Once the value of $D/\rho h$ is known, the parameter-based weights are determined. In Sec. IV, experimental results obtained using both averaged weights and parameter-based weights will be presented.

IV. EXPERIMENTAL RESULTS

A simply supported plate and a clamped plate were both assembled using 6061-T6 rolled aluminum, which had the same material properties and dimensions as the plate used in the simulations (see Table I). The simply supported boundary conditions were created by suspending the plate in a stiff frame with set screws the points of which touch the four sides of the plate, as shown in Fig. 7. The result of the set screws contacting the edges of the plate is that they prevent any transverse motion but allow rotation to provide a near simply supported boundary condition. The clamped boundary condition was created by placing the plate between two stiff frames and bolting the frames together. A picture of the clamped plate is also shown in Fig. 7. Spatially dense velocity measurements across the plates were made with a Polytec PSV-400 scanning laser Doppler vibrometer (SLDV) to confirm the intended boundary conditions were satisfied.

The plate was excited using a Labworks ET-126 shaker attached to a signal generator and controlled with a Bruel and Kjaer type 4809 vibration exciter. These shakers were suspended from a stiff frame with bungee cords and attached to the plate by gluing the individual stingers to the back side. WSSG was measured at a point on the front side using four accelerometers (PCB Model No. 352C68) spaced 0.0254 m apart in each direction,[32] as shown in Fig. 8.

Each of the terms in Eq. (14) was found numerically by calculating finite difference estimates of the derivatives from the accelerometer signals at each sampled time step. The equations used to calculate each term are

$$w \approx \frac{s_1 + s_2 + s_3 + s_4}{4}, \tag{17}$$

$$\frac{\partial w}{\partial x} \approx \frac{s_2 - s_1 + s_4 - s_3}{2\Delta x}, \tag{18}$$

$$\frac{\partial w}{\partial y} \approx \frac{s_1 - s_3 + s_2 - s_4}{2\Delta y}, \tag{19}$$

$$\frac{\partial^2 w}{\partial x \partial y} \approx \frac{s_2 - s_1 + s_3 - s_4}{\Delta x \Delta y}, \tag{20}$$

where s_i represents the instantaneous acceleration measured by each accelerometer, and Δx and Δy represent the x and y distance between the accelerometers, respectively, as shown in Fig. 8. Accelerations are used interchangeably with displacements with no impact on the result for minimizing WSSG. There is a trade-off for choosing the distance between the accelerometers, as discussed in greater detail in Hendricks et al.[32] If two accelerometers are placed too close, they may read almost the same value, even though in principle, closely spaced sensors are able to better approximate the derivatives in Eqs. (17)–(20). On the other hand, if accelerometers are placed too far apart, the values read from the accelerometers vary more, but the approximations in Eqs. (17)–(20) deteriorate in accuracy. In addition, the fourth term of WSSG shown in Eq. (20) has two orders of approximation; hence it has more numerical error than the other three terms. This fourth term has already been shown to have only a minor effect on the control performance in Sec. III.

The calculation of each WSSG term was accomplished within the DSP controller (based on the TI TMS C6713 processor), which implemented a modified filtered-x LMS algorithm to optimize the phase and amplitude of the
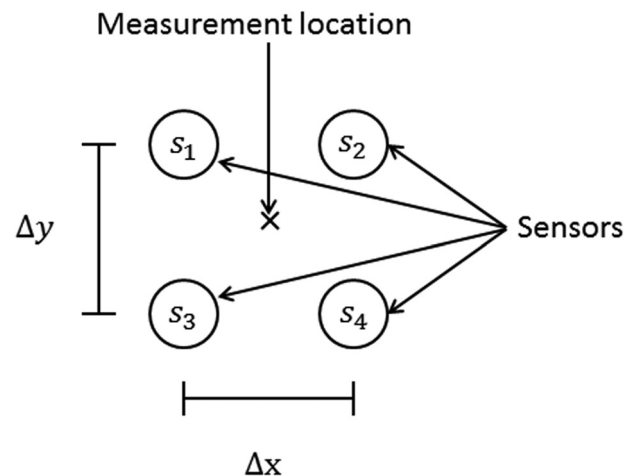

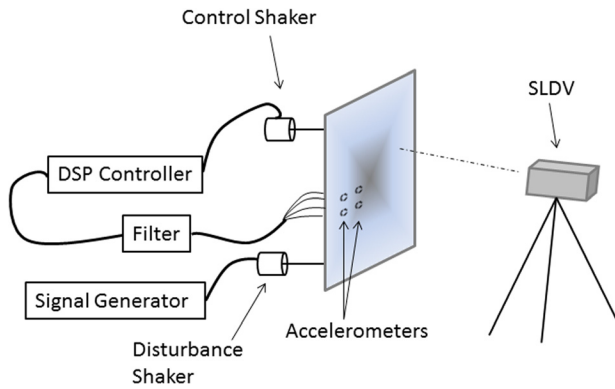FIG. 8. Schematic of accelerometer spacing used to measure WSSG.

FIG. 9. (Color online) Schematic of the experimental setup.

complex control force to minimize WSSG.[27] The sampling frequency was 4 kHz, and the convergence step size was adjusted for each frequency to achieve rapid and stable convergence. The SLDV was used to measure the velocity at an array of points on the plate, and then sound power was calculated using the method of elementary radiators used previously for the simulations. A full schematic of the experimental setup is shown in Fig. 9. To obtain accurate sound measurements, the plate was placed in a window between two acoustic reverberation chambers with the plate radiating into the chamber with dimensions 5.69 m × 4.32 m × 2.49 m. This provided a baffle between the two sides of the plate and isolated the plate from any outside vibrations or noises.

Averaged weights and parameter-based weights for WSSG were considered in the experimental work. Experimental averaged weights were obtained by averaging all of the weights corresponding to every mode in the frequency range of interest, below 500 Hz. The weights corresponding to each structural mode were chosen by making WSSG as uniform as possible over the entire surface of the plate. The parameter-based weights were obtained based on the value of $D/\rho h$.

A. Simply supported plate

In this section, the radiated sound power reduction obtained experimentally using averaged weights and parameter-based weights is compared for the simply supported plate. The actuator and sensor locations are the same as shown in Table II.

Figure 10 shows the comparison of control results between using averaged weights and parameter-based weights. Note that the frequency resolution for the experimental results is 10 Hz. It can be seen that significant attenuation is achieved from 40 to 200 Hz, which is consistent with the simulation results shown in Fig. 6(a). The two degenerate modes shown in Fig. 10 corresponding to the simulation results are at 232 and 339 Hz now at which minimal attenuation is achieved. In addition to the two degenerate modes, there is also little attenuation at 303 Hz using both averaged weights and parameter-based weights. The velocity response at 303 Hz was plotted and it was found to be another degenerate mode. At higher frequencies above 250 Hz, the experimental results using averaged weights did not result in good attenuation. This may be due to the large numerical noise that appears at higher frequencies due to the higher-order spatial derivative of the experimental data used to compute the fourth term in WSSG. The parameter-based weights do not use the fourth term, which may lead to the better control performance that is obtained at high frequencies.

Figure 10 also shows the comparison of the control results between averaged weights and parameter-based weights when using two control shakers. It can be seen that compared with using just one shaker, more attenuation is obtained at the degenerate mode frequency of 232 Hz using two shakers. In contrast with the simulation results, the degenerate modes at 339 Hz also experience some attenuation using two shakers; this may be affected by the additional loading effect of the shakers. At high frequencies, there is significantly better control performance achieved than when using just one shaker.

B. Clamped plate

The radiated sound power control results for the clamped plate are presented in this section. The actuator and sensor locations are the same as shown in Table II. Figure 11 shows the experimental comparison of the radiated sound
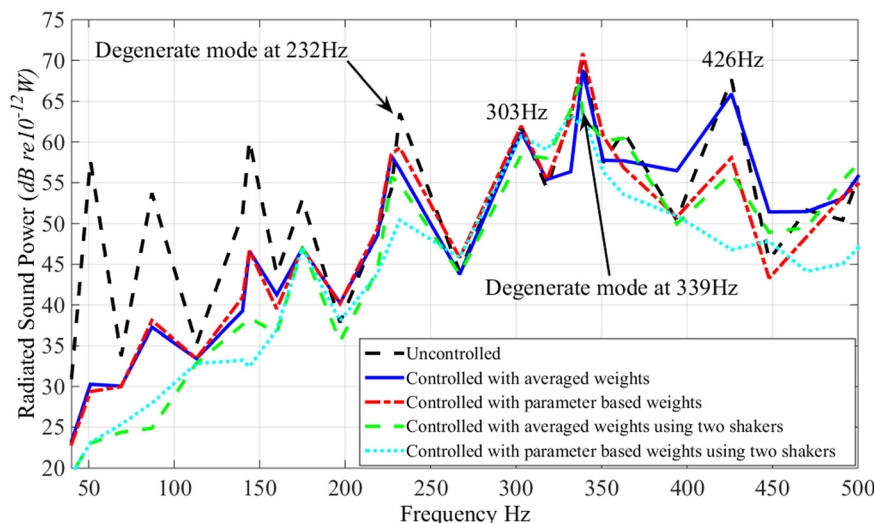

FIG. 10. (Color online) Experimental comparison of control results when using parameter-based weights and averaged weights for the simply supported plate.

J. Acoust. Soc. Am. **138** (5), November 2015
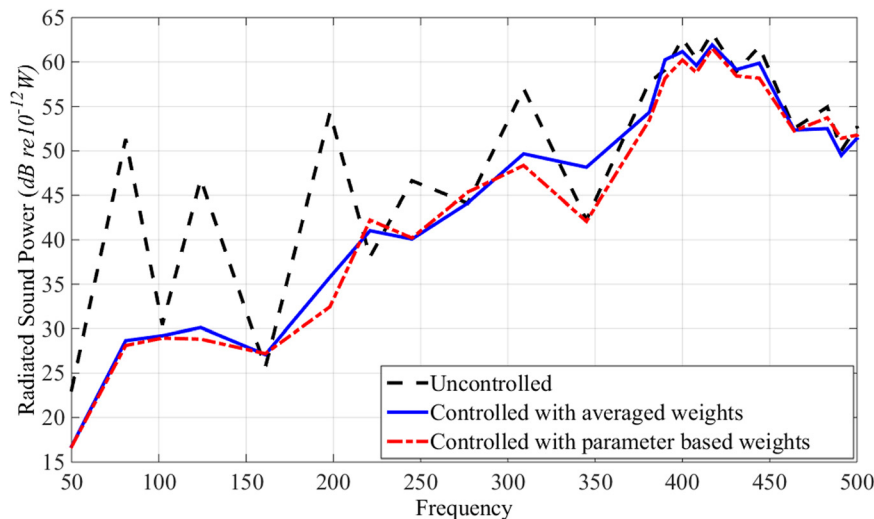
Cao *et al.* 2995

FIG. 11. (Color online) Experimental comparison of control results between parameter-based weights and averaged weights for the clamped plate.

power control results between parameter-based weights and averaged weights for the clamped plate. It can be seen that good attenuation is achieved across nearly the entire frequency range. Nearly the same attenuation is achieved for both averaged weights and parameter-based weights from 50 to 300 Hz. Averaged weights were not as effective in the region around 345 Hz; this is consistent with the simulation results from 350 to 400 Hz shown in Fig. 6(b). At relatively high frequencies, the averaged weights perform slightly worse than the parameter-based weights. This may be partially due to the noise inherent in the calculations by computing the higher order derivatives of the experimental data used in the fourth term of WSSG for averaged weights.

V. CONCLUSIONS

In this paper, WSSG has been shown numerically and experimentally to be an effective control metric for reducing the radiated sound power from simply supported and clamped plates. In implementing WSSG, it was found that the weights used have a direct relation with the control performance achieved. Numerical simulation demonstrated that optimizing the WSSG weights at each frequency using a simulated annealing process resulted in attenuation as good as the optimal, but impractical, approach of minimizing sound power. A more simple process than simulated annealing is preferable to find the optimized weights in real implementations. As a result, a method called parameter-based weights for broadband frequency ranges was developed and has been validated both numerically and experimentally. The parameter-based weights are directly related to the ratio of bending rigidity to area mass density ($D/\rho h$) of the plate, which is inversely proportional to the square of the flexural wavenumber. Both simulation and experimental results compared well and indicated that parameter-based weights can easily be obtained and provide significant control over relatively large frequency ranges.

ACKNOWLEDGMENT

[1]C. R. Fuller, "Analysis of active control of sound radiation from elastic plates by force inputs," in *Proceedings of Inter-Noise '88*, Avignon (1988), Vol. 2, pp. 1061–1064.
[2]C. R. Fuller, "Active control of sound transmission/radiation from elastic plates by vibration inputs. I: Analysis," J. Sound Vib. **136**, 1–15 (1990).
[3]B. T. Wang, C. R. Fuller, and E. K. Dimitriadis, "Active control of structurally radiated noise using multiple piezoelectric actuators," AIAA J. **29**(11), 1802–1809 (1991).
[4]C. R. Fuller, C. H. Hansen, and S. D. Snyder, "Active control of sound radiation from a vibrating panel by sound sources and vibration inputs: An experimental comparison," J. Sound Vib. **145**, 195–216 (1991).
[5]R. L. Clark and C. R. Fuller, "Experiments on active control of structurally radiated sound using multiple piezoceramic actuators," J. Acoust. Soc. Am. **91**, 3313–3320 (1992).
[6]C. R. Fuller, S. J. Elliott, and P. A. Nelson, *Active Control of Vibration* (Academic, London, 1997), pp. 223–251.
[7]J. Pan, S. D. Snyder, C. H. Hansen, and C. R. Fuller, "Active control of far field sound radiated by a rectangular panel: A general analysis," J. Acoust. Soc. Am. **91**, 2056–2066 (1992).
[8]S. D. Snyder and C. H. Hansen, "Mechanisms of active noise control using vibration sources," J. Sound Vib. **147**, 519–525 (1991).
[9]S. J. Elliott and M. E. Johnson, "Radiation modes and the active control of sound power," J. Acoust. Soc. Am. **94**, 2194–2204 (1993).
[10]M. E. Johnson and S. J. Elliott, "Active control of sound radiation using volume velocity cancellation," J. Acoust. Soc. Am. **98**, 2174–2186 (1995).
[11]M. E. Johnson and S. J. Elliott, "Active control of sound radiation from vibrating surfaces using arrays of discrete actuators," J. Sound Vib. **207**, 743–759 (1997).
[12]X. Pan, T. Sutton, and S. J. Elliott, "Active control of sound transmission through a double-leaf partition by volume velocity cancellation," J. Acoust. Soc. Am. **104**, 2828–2835 (1998).
[13]C. Maury, P. Gardonio, and S. J. Elliott, "Active control of the flow-induced noise transmitted through a panel," AIAA J. **39**, 1860–1867 (2001).
[14]P. Gardonio, Y. S. Lee, and S. J. Elliott, "Analysis and measurement of a matched volume velocity sensor and uniform force actuator for active structural acoustic control," J. Acoust. Soc. Am. **110**, 3025–3031 (2001).
[15]K. Henrioulle and P. Sas, "Experimental validation of a collocated PVDF volume velocity sensor/actuator pair," J. Sound Vib. **265**, 489–506 (2003).
[16]T. Sors and S. J. Elliott, "Volume velocity estimation with accelerometer arrays for active structural acoustic control," J. Sound Vib. **258**, 867–883 (2002).
[17]N. Tanaka, S. D. Snyder, and C. H. Hansen, "Distributed parameter modal filtering using smart sensors," J. Vib. Acoust. **118**, 630–640 (1996).
[18]B. S. Cazzolato and C. H. Hansen, "Active control of sound transmission using structural error sensing," J. Acoust. Soc. Am. **104**, 2878–2889 (1998).
[19]G. P. Gibbs, R. L. Clark, D. E. Cox, and J. S. Vipperman, "Radiation modal expansion: Application to active structural acoustic control," J. Acoust. Soc. Am. **107**, 332–339 (2000).
[20]S. D. Snyder and N. C. Burgan, "An acoustic-based modal filtering approach to sensing system design for active control of structural acoustic

radiation: Theoretical development," Mech. Syst. Signal Process. **16**, 123–139 (2002).

[21] J. P. Maillard and C. R. Fuller, "Advanced time domain wave-number sensing for structural acoustic systems. I. Theory and design," J. Acoust. Soc. Am. **95**, 3252–3261 (1994).

[22] J. P. Maillard and C. R. Fuller, "Advanced time domain wave-number sensing for structural acoustic systems. II. Active radiation control of a simply supported beam," J. Acoust. Soc. Am. **95**, 3262–3272 (1994).

[23] J. P. Maillard and C. R. Fuller, "Advanced time domain wavenumber sensing for structural acoustic systems. III. Experiments on active broadband radiation control of a simply supported plate," J. Acoust. Soc. Am. **98**, 2613–2621 (1995).

[24] Y. Feldman, A. Andrianov, E. Polygalov, I. Ermolina, G. Romanychev, and Y. Zurev, "Time domain dielectric spectroscopy: An advanced measuring system," Rev. Sci. Instrum. **67**, 3208–3216 (1996).

[25] T. Kaizuka and N. Tanaka, "Radiation clusters and the active control of sound transmission into a symmetric enclosure," J. Acoust. Soc. Am. **121**, 922–937 (2007).

[26] T. Kaizuka and N. Tanaka, "Radiation clusters and active control of sound transmission through symmetric structures into free space," J. Sound Vib. **311**, 160–183 (2008).

[27] J. M. Fisher, J. D. Blotter, S. D. Sommerfeldt, and K. L. Gee, "Development of a pseudo-uniform structural quantity for use in active structural acoustic control of simply supported plates: An analytical comparison," J. Acoust. Soc. Am. **131**, 3833–3840 (2012).

[28] S. S. Rao, *Vibration of Continuous Systems* (Wiley, Hoboken, NJ, 2007), pp. 457–484.

[29] A. W. Leissa, *Vibration of Plates* (Ohio State University, Columbus, OH, 1993), pp. 59–65.

[30] C.-C. Sung and C. T. Jan, "Active control of structurally radiated sound from plates," J. Acoust. Soc. Am. **102**, 370–380 (1997).

[31] F. Fahy and P. Gardonio, *Sound and Structural Vibration: Radiation, Transmission and Response* (Academic, New York, 2007).

[32] D. R. Hendricks, W. R. Johnson, S. D. Sommerfeldt, and J. D. Blotter, "Experimental active structural acoustic control of simply supported plates using a weighted sum of spatial gradients," J. Acoust. Soc. Am. **136**(5), 2598–2608 (2014).

J. Acoust. Soc. Am. **138** (5), November 2015

Cao *et al.* 2997